



1 **Exploring HONO production from particulate nitrate**
2 **photolysis in Chinese representative regions:**
3 **characteristics, influencing factors and environmental**
4 **implications**

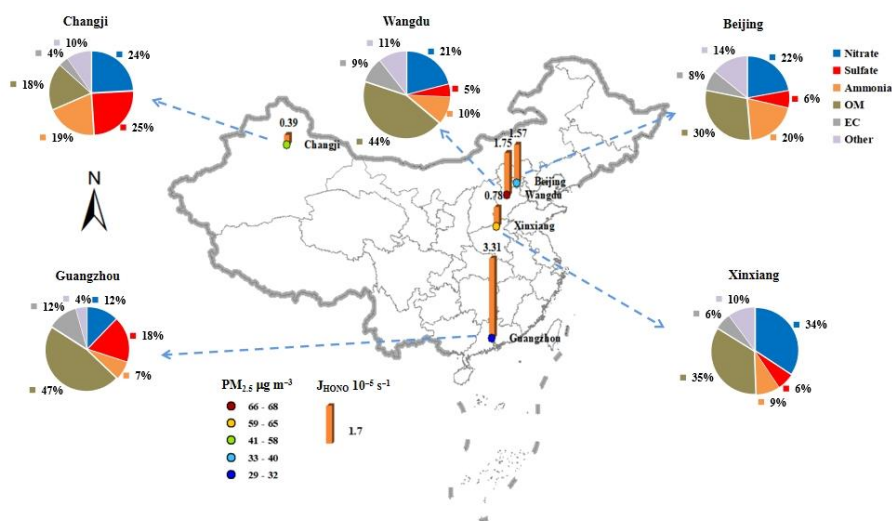
5 Bowen Li¹, Jian Gao¹, Chun Chen¹, Liang Wen¹, Yuechong Zhang¹, Junling Li¹,
6 Yuzhe Zhang¹, Xiaohui Du¹, Kai Zhang¹, Jiaqi Wang¹

7 ¹State Key Laboratory of Environmental Criteria and Risk Assessment, Chinese Research Academy of
8 Environmental Sciences, Beijing 100012, China

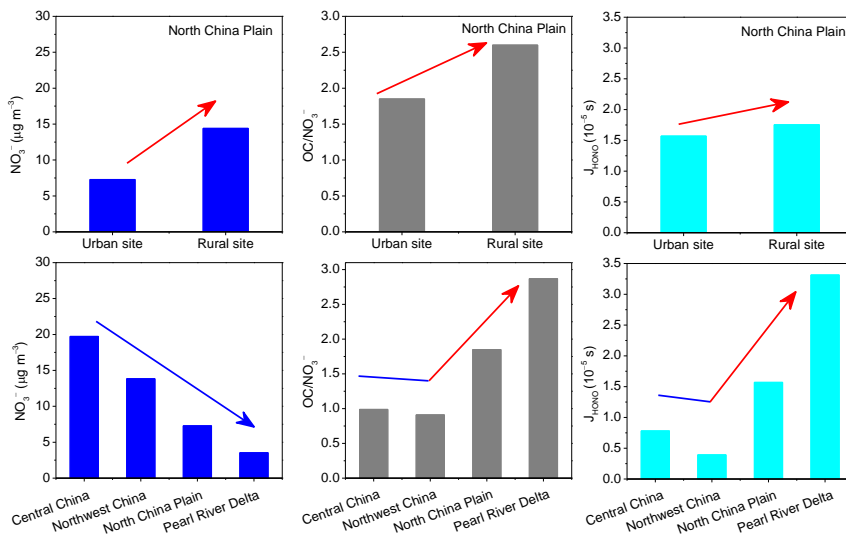
9 *Correspondence to:* Jiaqi Wang (wang.jiaqi@craes.org.cn), Kai Zhang (zhangkai@craes.org.cn)

10

11 **Abstract.** The production mechanism of atmospheric nitrous acid (HONO), an important precursor of
12 hydroxyl radical (OH), was still controversial. Few studies have explored the effects of particulate
13 nitrate photolysis on HONO sources in different environment conditions across China. Here, the
14 photolysis rate constants of particulate nitrate for HONO production (J_{HONO}) were determined through
15 photochemical reaction system with $\text{PM}_{2.5}$ samples collected from five representative sites in China. To
16 eliminate the “shadowing effect” — potential light extinction within aerosol layers at heavy $\text{PM}_{2.5}$
17 loadings on the filters, the relationship between light screening coefficient and EC, the dominant
18 light-absorbing component in $\text{PM}_{2.5}$, was established ($R^2=0.73$). The corrected J_{HONO} values varied with
19 sampling period and location over a wide range, distributing from $1.6 \times 10^{-6} \text{ s}^{-1}$ to $1.96 \times 10^{-4} \text{ s}^{-1}$, with a
20 mean ($\pm 1 \text{ SD}$) of $(1.71 \pm 2.36) \times 10^{-5} \text{ s}^{-1}$. Chemical compositions, specifically nitrate loading and
21 organic component, affected the production of HONO through particulate nitrate photolysis: high J_{HONO}
22 values were generally associated with the $\text{PM}_{2.5}$ samples with high OC/NO_3^- ratio ($R^2=0.86$). We
23 suggested that the parameterization equation between J_{HONO} and OC/NO_3^- established in this
24 work can be used to estimate J_{HONO} in different aerosol chemical conditions, thus reducing the
25 uncertainty in exploring HONO daytime sources. This study confirms that the photolysis of
26 particulate nitrate can be a potential HONO daytime source in rural or southern urban sites,
27 which were characterized by high proportion of organic matter in $\text{PM}_{2.5}$, while the contribution
28 of this process to HONO daytime formation was still limited.



29



30



31 **1 Introduction**

32 Gaseous nitrous acid (HONO) is an important nitrogen-containing trace gas in the troposphere,
33 which can produce hydroxyl radical (OH) through photolysis, thus stimulating the enhancement of
34 atmospheric oxidation and the formation of secondary aerosols (Fu et al., 2019; Slater et al., 2020; Ren
35 et al., 2003; Li et al., 2011; Su et al., 2011). In recent years, the contribution of HONO to atmospheric
36 oxidation in heavily polluted conditions has attracted great attention (Villena et al., 2011; Fu et al.,
37 2019; Slater et al., 2020). Even though observational research on HONO has been conducted for nearly
38 40 years, the understanding of HONO daytime source was still controversial (Fu et al., 2019; Wang et
39 al., 2017; Mora Garcia et al., 2021). Numerous mechanisms have been proposed to explain the
40 extremely high HONO concentrations at noon, including direct combustion emission (Kurtenbach et al.,
41 2001; Liang et al., 2017; Liao et al., 2021), gas-phase reaction of NO and OH radical (Li et al., 2011;
42 Zhang et al., 2016), heterogeneous reaction of NO₂ (Wang et al., 2017; Ammann et al., 1998; Monge et
43 al., 2010; Stemmler et al., 2006), soil emissions (Su et al., 2011; Oswald et al., 2013; Melissa A, 2014;
44 Kim and Or, 2019), and the photolysis of HNO₃/nitrate on aerosol or ground surface (Zhou et al., 2003;
45 Zhou et al., 2011; Ye et al., 2016b; Ye et al., 2016a; Ye et al., 2017).

46 Particulate nitrate, which was conventionally considered as the ultimate oxidation product of NO_x,
47 can rapidly photolyze and recycle NO_x or HONO back to the gas phase (Andersen et al., 2023; Handley
48 et al., 2007; Beine et al., 2006; Ye et al., 2016a; Ye et al., 2017; Ye et al., 2016b; Gu et al., 2022b), at a
49 rate 10 to 300 times faster than the photolysis rate of gaseous HNO₃ ($\sim 7 \times 10^{-7} \text{ s}^{-1}$) under typical
50 tropical noontime conditions (Finlayson-Pitts, 2000). Recently, some field, laboratory and modeling
51 works have proposed that photolysis of particulate nitrate can be an important in situ source of HONO
52 in rural, suburban and urban environments (Ye et al., 2016b; Mora Garcia et al., 2021; Liu et al., 2019;
53 Bao et al., 2018; Wang et al., 2017). Fu et al. (2019) found that the photolysis of HNO₃/nitrate in the
54 atmosphere and deposited on surfaces was the dominant HONO source during noon and afternoon,
55 contributing above 50 % of the simulated HONO. However, there are large discrepancies in estimating
56 the rate constants in the atmosphere (Gen et al., 2022). In New York, Ye et al. (2017) reported that the
57 photolysis rates of particulate nitrate in clean areas were two orders of magnitude higher than that in
58 polluted areas, ranging from 6.2×10^{-6} to $5.0 \times 10^{-4} \text{ s}^{-1}$, with a median of $8.3 \times 10^{-5} \text{ s}^{-1}$. The proposed rate
59 constants of nitrate photolysis based on the aircraft observations over South Korea ranged from 7×10^{-6}



60 to $2.1 \times 10^{-5} \text{ s}^{-1}$ (Romer et al., 2018). Shi et al. (2021) derived the rate constant ($< 2 \times 10^{-5} \text{ s}^{-1}$) based on
61 chamber experiments, but found a limited role of this mechanism to HONO production. The
62 uncertainty of HONO production rate from the photolysis of particulate nitrate can reach up to 1.4 ppbv
63 h^{-1} , and greatly affect the accuracy of HONO source analysis (Liu et al., 2019; Lee et al., 2016; Ye et
64 al., 2016a). The highly-varied photolysis rate constant of particulate nitrate was closely associated with
65 environmental conditions and the aerosol chemical or physical characteristics, such as relative humidity
66 (RH), aerosol acidity, light intensity, and coexisting components (organic components, halogen, etc.)
67 (Gelencsér et al., 2003; Ye et al., 2016a; Bao et al., 2020; Wang et al., 2021; Reeser et al., 2013). Thus,
68 elucidating the mechanism and dominant factors controlling the photolysis of particulate nitrate is
69 important to accurately estimate the contribution of this process to HONO daytime production.

70 In general, the photolysis rate constant of particulate nitrate was derived through photochemical
71 experiments using bulk particle samples collected on filters (Ye et al., 2017; Bao et al., 2018).
72 Comparing with the suspended particles in the ambient atmosphere, the collected $\text{PM}_{2.5}$ particles in the
73 aerosol filters may present a multiple-layer structure, especially in heavy air pollution conditions (Bao
74 et al., 2018). The light-absorbing species within $\text{PM}_{2.5}$ particles would hinder the light absorption of
75 particulate nitrate in the lower layers of the filter sample, thus inhibiting the photolysis of particulate
76 nitrate, which was called the “shadowing effect” (Ye et al., 2017). The shadowing effect may be
77 negligible in clean air conditions but should be evaluated and quantified in heavy haze conditions.
78 However, previous works generally ignored this shadowing effect.

79 According to previous field observations, the $\text{PM}_{2.5}$ chemical composition, especially particulate
80 nitrate concentration (NO_3^-), changed significantly across China (Wang et al., 2022a, b; Wang et al.,
81 2022c; Wang et al., 2016; Cheng et al., 2024). As one of the key industrial development areas in China,
82 the Pearl River Delta Region (PRD) has a great number of large-scale industrial parks dominated by the
83 chemical industry, resulting in significant VOC emissions and a large proportion of organic matter (OM)
84 in $\text{PM}_{2.5}$. In the North China Plain (NCP), the particulate nitrate (NO_3^-) has surpassed sulfate (SO_4^{2-})
85 and OM to become the dominant $\text{PM}_{2.5}$ component in recent years (Wang et al., 2022b). For now, the
86 investigation of particulate nitrate photolysis in different atmospheric environments was limited in
87 China, and the influence of aerosol chemical or physical characteristics on HONO production was still
88 unclear. In this work, to shed light on the contribution of particulate nitrate photolysis to the HONO
89 daytime source, we examined the photolysis rate constant for HONO based on photochemical



90 experiments with $PM_{2.5}$ samples collected from five typical sites in China. In addition, the shadowing
91 effect due to increasing aerosol particle loading on the filters was quantified. After correcting this effect,
92 the influence of various environmental conditions, including particulate nitrate, organic matter, and
93 aerosol acidity, on the formation of HONO was investigated and the possible role of this photolytic
94 process as HONO sources was also examined.

95 **2 Method**

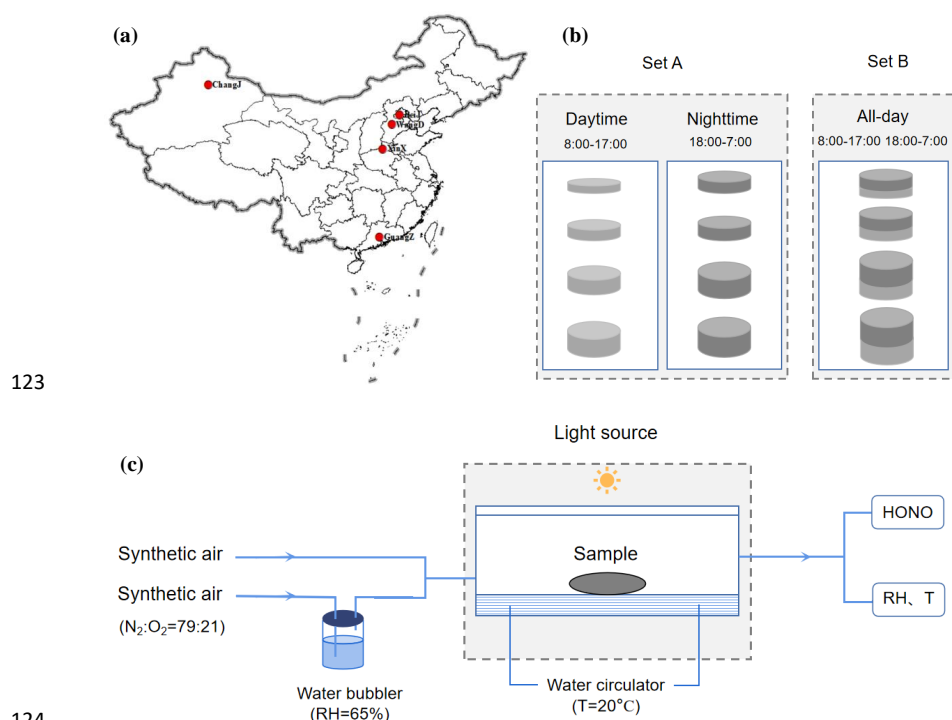
96 **2.1 Sampling and filter treatment**

97 The ambient $PM_{2.5}$ was collected on Teflon or quartz filters in autumn-winter seasons in five
98 representative sites, i.e., Beijing, Wangdu, Xinxiang, Guangzhou, and Changji, which were shown in
99 Figure 1a and described in detail in the Supporting Information. These cities were located in the North
100 China Plain (NCP, urban: Beijing, rural: Wangdu), Central China, Pearl River Delta Region (PRD), and
101 Northwestern China, respectively. The sampling flow rates ranged from 16.7 to 1050 L min^{-1} , the
102 sampling times from 9 h to 23 h, and the overall sampling volumes of air from 8 m^3 to 1450 m^3 , to
103 collect a very wide range of particulate nitrate loadings. The comparison experiments between Teflon
104 and quartz filters have been conducted, and no significant differences in HONO production rates from
105 particulate nitrate photolysis have been found ($T < 0.01$). The sampling settings employed in Wangdu
106 were designed to quantify the shadowing effect (Figure 1b). In Wangdu, $PM_{2.5}$ was collected at a flow
107 rate of 16.7 L min^{-1} with four channels (A, B, C, and D). A and B channels were set for
108 daytime (8:00–17:00) and nighttime (18:00–7:00) $PM_{2.5}$ samples, respectively, and the other two
109 channels were for the “all-day” (including 8:00–17:00 and 18:00–7:00) $PM_{2.5}$ samples. A total of 158
110 effective $PM_{2.5}$ samples were obtained in this study. These aerosol filter samples were labeled and
111 stored at $-20\text{ }^{\circ}C$ in the freezer.

112 Fractions with given surface area from each filter sample were used to perform photochemical
113 reaction experiments and analysis of aerosol chemical components. For each $PM_{2.5}$ sample, the fraction
114 with given surface area was rinsed by deionized water and then sonicated for 15 min. The amounts of
115 water-soluble ions including Na^+ , NH_4^+ , K^+ , Mg^{2+} , Ca^{2+} , Cl^- , NO_3^- , and SO_4^{2-} were measured by ion
116 chromatography (IC, Thermo ICS-2100). To measure the values of carbon components, including
117 organic carbon (OC) and elemental carbon (EC), a part ($0.5024\text{ }cm^2$) of each filter was detected using a



118 thermal optical carbon analyzer (DRI model 2015). The concentration of OM was obtained by
 119 multiplying the OC concentration by a factor of 1.6 (Li et al., 2021). $PM_{2.5}$ concentration was estimated
 120 by the sum of all the water-soluble ions and carbon components. The surface concentration of $PM_{2.5}$
 121 and its components on aerosol filters were calculated through dividing the absorbed loading with the
 122 geometric area of the aerosol filter sample ($\mu g\ cm^{-2}$).



123

124

125 **Figure 1.** (a) Location map of five representative sampling sites in China, (b) the sampling settings to
 126 quantify the shadowing effect in Wangdu, and (c) a schematic diagram of the photochemical
 127 experimental setup.

128 2.2 Photochemical reaction system

129 A custom-made cylindrical quartz vessel was used as the photochemical flow reactor (Figure 1c).
 130 The diameter was 10 cm and the depth was 2.5 cm, with a cell volume of ~200 ml. A xenon lamp (300
 131 W) was placed 20 cm above the reactor as the light source. The light was filtered by a Pyrex sleeve to
 132 remove heat-generating infrared light. The effective light intensity in the center of the flow reactor,
 133 where aerosol samples were placed, was measured to be about 0.5 times higher ($1.5\ kW\ m^{-2}$, measured



134 by a calibrated optical power meter) than that at tropical noon on the ground (solar elevation angle
135 $\theta=0^\circ$). Synthetic air, composed of ultrahigh-purity nitrogen and ultrahigh-purity oxygen mixed at a
136 ratio of 79:21, was used as the carrier gas. The relative humidity (RH) in the air flow was adjusted
137 through a water bubbler and monitored with an online RH sensor (Vaisala, HMT130). The aerosol filter
138 sample was exposed to the solar simulator radiation for 20 min. The photochemical reaction
139 experiment for each sample was repeated 2–3 times with different fractions from the same sample. The
140 gaseous product (i.e., HONO) released during the experiment was flushed out of the reactor by the
141 carrier gas and was detected online by a custom-built HONO analyzer, which had been applied in
142 several measurements previously (Zhang et al., 2020b; Li et al., 2021).

143 2.3 HONO Production from the photolysis of particulate nitrate

144 The production rates (nmol h^{-1}) of HONO from particulate nitrate photolysis (P_{HONO}) were
145 calculated from their time-integrated signals above the baselines over the period of light exposure:

$$146 P_{\text{HONO}} = \frac{F_g \times 60}{V_m(t_2 - t_1)} \int_{t_1}^{t_2} C_{\text{HONO}} dt \quad (1)$$

147 Where F_g (L min^{-1}) is the flow rate of the carrier gas, V_m (24.5 L mol^{-1}) is the molar volume of gas at
148 25°C and 1 atm of pressure; t_1 and t_2 (min) are the starting and ending time of the irradiation,
149 respectively; C_{HONO} (ppb) is the online measured concentration of HONO. With the flow rate of 2.5 L
150 min^{-1} , the residence time in the reaction system was around $\sim 5 \text{ s}$. The photolytic loss of HONO was
151 less than 5 %, thus no correction was made in the calculation of HONO production.

152 The photolysis rate constant of particulate nitrate leading to HONO production ($J_{\text{HONO}}, \text{ s}^{-1}$) was
153 calculated by the following equation:

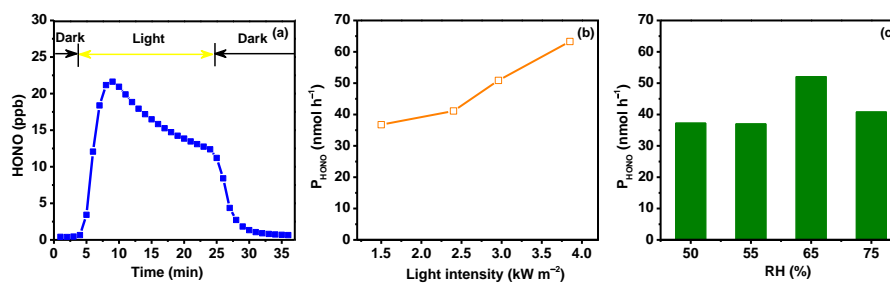
$$154 J_{\text{HONO}} = \frac{P_{\text{HONO}}}{N_{\text{NO}_3^-} \times 3600} \quad (2)$$

155 Where $N_{\text{NO}_3^-}$ (mol) is the amount of NO_3^- in the tested $\text{PM}_{2.5}$ sample. In principle, the photolysis rate
156 constant should be calculated on the amount of NO_3^- that is reachable to the irradiation. However, the
157 amount of the light-reachable NO_3^- in the $\text{PM}_{2.5}$ sample was hard to quantify. In this work, the
158 deviation of J_{HONO} due to the overestimate of the amount of NO_3^- under light irradiation, which was
159 called the shadowing effect, would be corrected in Sect. 3.1.

160 3 Results



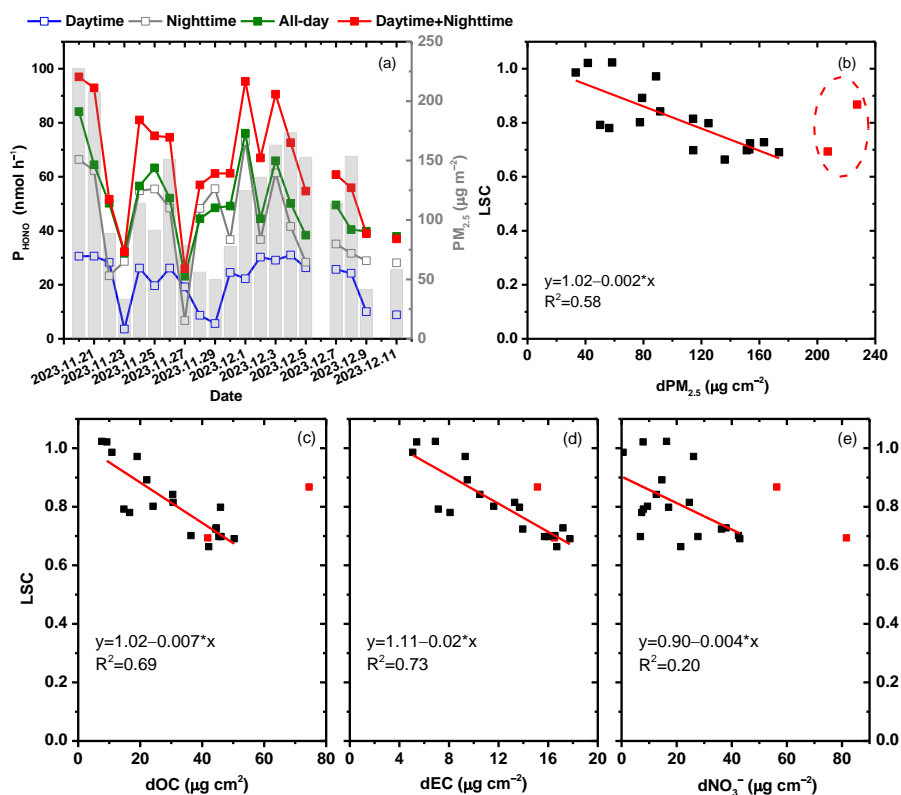
161 **3.1 Quantify the influence of the shadowing effect**



162

163 **Figure 2.** (a) Online measured concentrations of HONO during the light-exposure of an aerosol sample
 164 collected on June 12, 2023 in Beijing, P_{HONO} as a function of (b) light intensity (kW m⁻²) and (c) RH
 165 (%).

166 HONO production within the first 20 min of irradiation during the photochemical experiment was
 167 investigated on the PM_{2.5} samples collected from five typical sites in China. Figure 2a showed a typical
 168 profile of the changes in HONO concentration in the reaction system. When the light was turned on,
 169 HONO concentration in the reactor increased immediately, then leveled off and slightly decayed
 170 afterwards. After the light was turned off, the HONO generation stopped immediately and the signal
 171 nearly returned to the baseline level. Previous works have revealed that the decay of HONO generation
 172 during light exposure period was not resulted from the evaporation loss of particulate nitrate (Ye et al.,
 173 2017), but mainly related to the inhomogeneity of particulate nitrate photochemical reactivity or the
 174 consumption of reactive electron donors, such as acidic proton (Bao et al., 2018). HONO production
 175 from the photochemical reactions of particulate nitrate were significantly influenced by ambient
 176 environmental conditions (i.e., light intensity and RH). As shown in Figure 2b, with the increase of
 177 light intensity, P_{HONO} gradually increased, with P_{HONO} in 3.85 kW m⁻² approximately twice than that in
 178 1.50 kW m⁻². Previous works found that the formation of HONO was negligible at low RH (<5%), and
 179 increased at intermediate RH (15%–75%), then turned to decrease at RH > 90% (Bao et al., 2018).
 180 Here, we found that P_{HONO} climbed to its highest when RH was around 65 % (Figure 2c). In this work,
 181 the photochemical reactions on different aerosol samples were all conducted under the same
 182 environmental condition (RH=65 %, temperature=20 °C, and light intensity=1.50 kW m⁻²).



183

184

185 **Figure 3.** (a) Temporal variation of P_{HONO} for aerosol filters collected in Wangdu during daytime,
 186 nighttime and all-day from November 20, 2023 to December 11, 2023, (b)-(e) relationships between
 187 light screening coefficient (LSC) and the surface concentrations of $\text{PM}_{2.5}$ ($d\text{PM}_{2.5}$), OC ($d\text{OC}$), EC ($d\text{EC}$)
 188 and NO_3^- ($d\text{NO}_3^-$), respectively. The red squares represent the aerosol samples with $\text{PM}_{2.5}$ surface
 189 concentration higher than $200 \mu\text{g cm}^{-2}$.

190 As expected, P_{HONO} increased with particulate nitrate loadings in different sampling locations
 191 (Figure S1), however, it's interesting to note that, P_{HONO} dose not increase or somewhat decrease at very
 192 high NO_3^- loading condition. Previous works considered this may be attributed to the shadowing effect,
 193 wherein the particulate nitrate underneath the aerosol filters may receive less UV light at heavy aerosol
 194 particle loading on the filters, inhibiting the photolysis of particulate nitrate (Ye et al., 2017). Thus, the
 195 reported P_{HONO} values would be underestimated under polluted ambient conditions. To verify and
 196 quantify the underestimation of P_{HONO} due to the shadowing effect, we collected two sets of filters in
 197 Wangdu (set A: daytime and nighttime, set B: all-day, Figure 1b). Theoretically, the all-day one should
 198 share the same NO_3^- loading and chemical composition as the sum of the daytime and nighttime filters,



199 thus the sum of P_{HONO} during daytime ($P_{\text{daytime}}^{\text{HONO}}$) and nighttime ($P_{\text{nighttime}}^{\text{HONO}}$) should be equal to that
200 during all-day ($P_{\text{all-day}}^{\text{HONO}}$) without considering the shadowing effect. A total of 20 pairs of comparative
201 photochemical experiments were conducted, and the comparison of P_{HONO} between these two sets of
202 filters was shown in Figure 3a. We found that the discrepancy between $P_{\text{all-day}}^{\text{HONO}}$ and $P_{\text{daytime}}^{\text{HONO}} +$
203 $P_{\text{nighttime}}^{\text{HONO}}$ was widening along with the increase of surface $\text{PM}_{2.5}$ concentration. To quantify the
204 shadowing effect, we introduced a parameter called “light screening coefficient” (LSC) to describe the
205 decreasing efficiency of light penetrating into the particle with increasing $\text{PM}_{2.5}$ loadings:

$$206 \quad P_{\text{theory}}^{\text{HONO}} = P_{\text{daytime}}^{\text{HONO}} + P_{\text{nighttime}}^{\text{HONO}} \quad (3)$$

$$207 \quad \text{LSC} = P_{\text{observed}}^{\text{HONO}} / P_{\text{corrected}}^{\text{HONO}} = P_{\text{all-day}}^{\text{HONO}} / P_{\text{theory}}^{\text{HONO}} \quad (4)$$

208 As shown in Figure 3b, when $\text{PM}_{2.5}$ surface concentration ($d\text{PM}_{2.5}$) was low, LSC was almost
209 equal to 1, indicating that the shadowing effect was negligible. With the increase of $\text{PM}_{2.5}$ loading, the
210 value of LSC declined to lower than 65 %. In general, significant negative correlation existed between
211 LSC and $d\text{PM}_{2.5}$, except when $d\text{PM}_{2.5}$ was higher than $200 \mu\text{g cm}^{-2}$ (Figure 3b). In this experiment, we
212 assumed that the daytime and nighttime $\text{PM}_{2.5}$ samples were both single-layered. However, with the
213 increase of air pollution, these filters in each pair of comparative experiments may already have
214 exhibited the shadowing effect, thus the sum of $P_{\text{daytime}}^{\text{HONO}}$ and $P_{\text{nighttime}}^{\text{HONO}}$ would be underestimated.
215 Therefore, when quantifying the shadowing effect, the LSC data with $\text{PM}_{2.5}$ loading higher than $200 \mu\text{g}$
216 cm^{-2} was excluded. Correlations between LSC and the surface concentrations of $\text{PM}_{2.5}$ major chemical
217 components, such as EC (dEC), OC (dOC), and NO_3^- ($d\text{NO}_3^-$), were conducted (Figure 3c-e).
218 Significant correlation was found between LSC and carbonaceous component, especially EC ($R^2=0.73$),
219 which was one of the most important light absorbing species in $\text{PM}_{2.5}$, indicating that the shadowing
220 effect was mainly related to the light absorption components in $\text{PM}_{2.5}$. The relationship between LSC
221 and dEC was established as following:

$$222 \quad d\text{EC} > 5.5 \mu\text{g m}^{-2}: \text{LSC} = 1.11 - 0.02 \times d\text{EC}$$

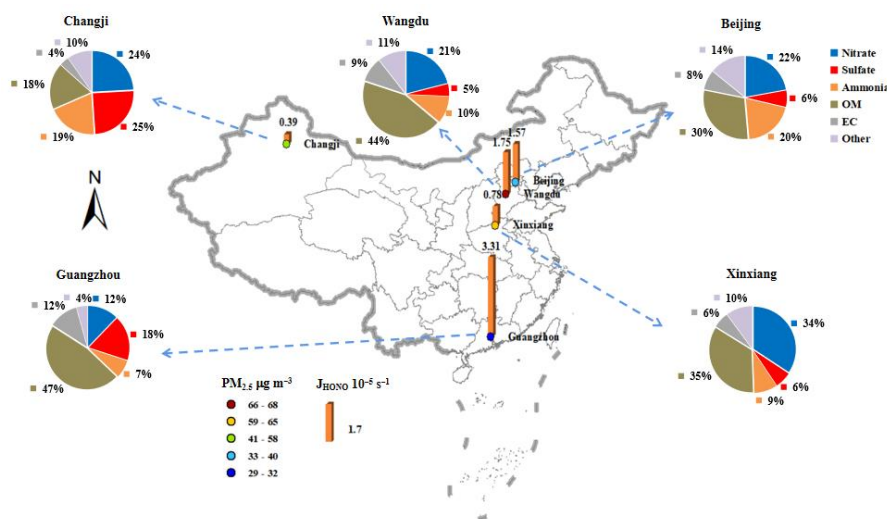
$$223 \quad d\text{EC} \leq 5.5 \mu\text{g m}^{-2}: \text{LSC} = 1 \quad (5)$$

224 when $d\text{EC} \leq 5.5 \mu\text{g m}^{-2}$, the shadowing effect can be ignored; when $d\text{EC} > 5.5 \mu\text{g m}^{-2}$, P_{HONO} can be
225 corrected by the observed P_{HONO} and LSC, which was estimated using this fitting equation with dEC.
226 Previous works found that the heavy loads of carbonaceous particles can turn these filters into dark
227 brown colors. The UV light was unlikely to transmit efficiently through the dark layer to the particulate
228 nitrate underneath, thus inhibiting the generation of HONO from the photolysis of particulate nitrate



229 (Ye et al., 2017). In consideration of the potential shadowing effect for the daytime and nighttime filters
 230 in each pair of comparative experiments, the $P_{\text{daytime}}^{\text{HONO}}$ and $P_{\text{nighttime}}^{\text{HONO}}$ observed would be
 231 underestimated, and the uncertainty of LSC should be considered at high $\text{PM}_{2.5}$ loadings. To evaluate
 232 this uncertainty, the observed $P_{\text{daytime}}^{\text{HONO}}$ and $P_{\text{nighttime}}^{\text{HONO}}$ values were recalculated and corrected to the
 233 theoretical single-layered condition based on Eq. (4) and (5). As shown in Figure S2, with the increase
 234 of $\text{PM}_{2.5}$ surface concentration, the deviations between LSC and the corrected one have enlarged.
 235 However, it's noted that the deviation was still lower than 20 % when $\text{PM}_{2.5}$ surface concentration was
 236 around $200 \mu\text{g cm}^{-2}$. For example, for the aerosol sample collected in December 4, 2023, in Wangdu,
 237 the $\text{PM}_{2.5}$ surface concentration was $173.57 \mu\text{g cm}^{-2}$, and the deviation was 15.74 %, which was
 238 acceptable in this work.

239 **3.2 Spatial distribution and temporal variation of HONO production from particulate nitrate**
 240 **photolysis**



241
 242 **Figure 4.** Spatial distribution of the average J_{HONO} , $\text{PM}_{2.5}$ loading, and chemical composition of the
 243 aerosol filters collected from five representative cities in China during the observation period.

244 There were 158 filter samples collected from five representative cities in China, and the averaged
 245 concentrations of $\text{PM}_{2.5}$ and its chemical composition of these filters showed significant spatial
 246 characteristics as shown in Figure 4. During the sampling period, OM was the most abundant species in
 247 $\text{PM}_{2.5}$ over most regions, except in the northwestern city (Changji), and NO_3^- was the dominant
 248 inorganic component in the NCP (Beijing and Wangdu) and Central China (Xinxiang), while SO_4^{2-}



249 showed the highest contribution in the PRD (GuangZ) and Northwestern China (Changji). The values
 250 of J_{HONO} on these $\text{PM}_{2.5}$ samples were calculated by Eq. (2) with the P_{HONO} corrected by Eq. (4) and (5),
 251 and summarized in Figure 4 and Table 1. The corrected J_{HONO} , median and mean (\pm one standard
 252 deviation), were $1.55 \times 10^{-5} \text{ s}^{-1}$ and $1.57 (\pm 2.14) \times 10^{-5} \text{ s}^{-1}$ in Beijing, $1.68 \times 10^{-5} \text{ s}^{-1}$ and $1.75 (\pm 2.83)$
 253 $\times 10^{-5} \text{ s}^{-1}$ in Wangdu, $0.69 \times 10^{-5} \text{ s}^{-1}$ and $0.78 (\pm 0.48) \times 10^{-5} \text{ s}^{-1}$ in Xinxiang, $3.04 \times 10^{-5} \text{ s}^{-1}$ and 3.31
 254 $(\pm 1.15) \times 10^{-5} \text{ s}^{-1}$ in Guangzhou, and $0.38 \times 10^{-5} \text{ s}^{-1}$ and $0.39 (\pm 0.25) \times 10^{-5} \text{ s}^{-1}$ in Changji, respectively.
 255 The maximum J_{HONO} in these cities ranged from $0.91 \times 10^{-5} \text{ s}^{-1}$ in Changji to $1.96 \times 10^{-4} \text{ s}^{-1}$ in Wangdu.
 256 These values were in the comparable range to those previously reported for aerosol samples, such as
 257 $1.22 \times 10^{-5} \text{ s}^{-1} \sim 4.84 \times 10^{-4} \text{ s}^{-1}$ in China by Bao et al. (2018) and 6.2×10^{-6} to $5.0 \times 10^{-4} \text{ s}^{-1}$ in US by Ye et
 258 al. (2017). It's interesting to note that the average J_{HONO} was the highest in Guangzhou, which was
 259 characterized with the lowest $\text{PM}_{2.5}$ and NO_3^- concentration among these cities. As for other cities with
 260 high $\text{PM}_{2.5}$ concentrations, such as Changji and Xinxiang, the corrected J_{HONO} was comparatively lower.
 261 According to the National Ambient Air Quality Standard of China (GB3095-2012), the daily $\text{PM}_{2.5}$
 262 averages in Guangzhou can meet the Level II standard of $75 \mu\text{g m}^{-3}$, while exceeding the level I
 263 standard ($35 \mu\text{g m}^{-3}$). Here, we defined $\text{PM}_{2.5}$ polluted days with daily mean $\text{PM}_{2.5}$ exceeding $35 \mu\text{g m}^{-3}$.
 264 As shown in Figure 5, the distribution of the corrected J_{HONO} values in clean days were generally more
 265 dispersed and higher than those in polluted days, except in Guangzhou. The average value of J_{HONO} in
 266 Guangzhou during air polluted conditions was slightly higher than that in clean conditions, besides
 267 much higher than the values in other cities. Because the influence of the shadowing effect has been
 268 corrected to some degree, these spatial and temporal change characteristics of J_{HONO} in this work should
 269 be mainly related to the varied chemical and physical properties of $\text{PM}_{2.5}$ samples collected from
 270 different atmospheric environments.

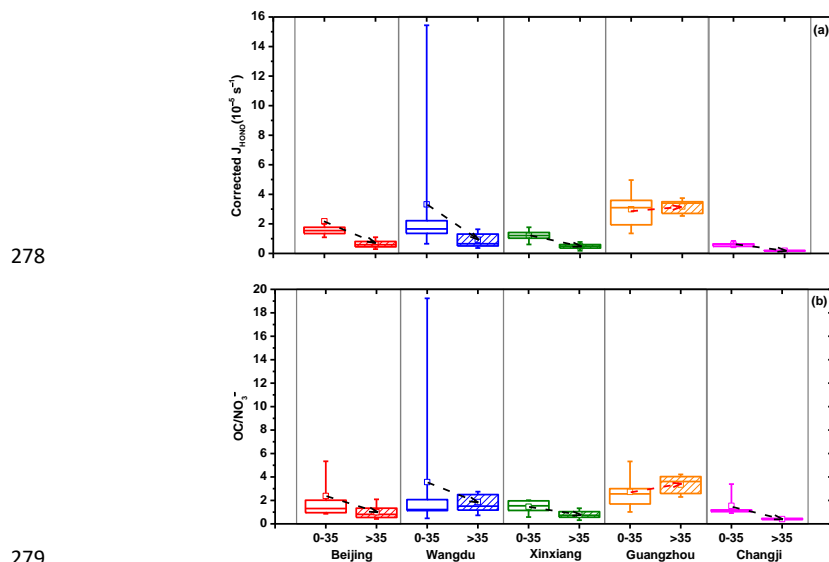
271 **Table 1.** The concentrations of $\text{PM}_{2.5}$ chemical composition, corrected J_{HONO} , and S_{HONO} in five
 272 representative cities in China under different air conditions during the sampling period.

Site	Air condition	$\text{PM}_{2.5}$ ($\mu\text{g m}^{-3}$)	NO_3^- ($\mu\text{g m}^{-3}$)	OC ($\mu\text{g m}^{-3}$)	OC/NO_3^-	Corrected J_{HONO} (10^{-5} s^{-1}) ^a	S_{HONO} ($10^{-5} \text{ mol h}^{-1} \text{ m}^{-2}$) ^b	S_{HONO} (ppbv h^{-1}) ^c
Beijing	Clean	19.71	3.15	3.89	2.25	2.01	0.15	0.03
	Polluted	72.56	19.71	12.62	0.87	0.61	0.38	0.09
	Whole-Min	4.32	0.08	1.07	0.32	0.21	0.04	0.01
	Whole-Max	102.64	32.90	15.95	12.82	11.06	0.57	0.13
	Whole-Mean	32.92	7.29	6.07	1.85	1.57	0.22	0.05



Changji	Clean	20.39	3.05	3.61	1.66	0.65	0.07	0.02
	Polluted	80.49	20.59	8.35	0.44	0.21	0.16	0.04
	Whole-Min	14.45	0.88	2.69	0.28	0.16	0.03 ^d	0.01 ^d
	Whole-Max	169.35	28.28	14.34	3.65	0.91	0.22	0.05
	Whole-Mean	57.37	13.84	6.53	0.91	0.39	0.13	0.03
Guangzhou	Clean	25.62	3.29	6.89	2.72	3.25	0.36	0.08
	Polluted	40.32	4.38	13.82	3.35	3.53	0.59	0.13
	Whole-Min	14.77	0.85	3.67	0.82	1.37	0.17	0.04
	Whole-Max	42.74	6.63	15.62	8.05	5.83	0.75	0.17
	Whole-Mean	29.12	3.55	8.54	2.87	3.31	0.41	0.09
Wangdu	Clean	22.16	3.29	5.36	4.79	3.80	0.20	0.04
	Polluted	83.53	18.06	23.23	1.88	1.09	0.50	0.11
	Whole-Min	10.67	0.24	2.72	0.22	0.23	0.06	0.01
	Whole-Max	173.45	60.28	63.07	22.06	19.60	0.88 ^e	0.20 ^e
	Whole-Mean	68.38	14.41	18.82	2.60	1.75	0.42	0.10
Xinxiang	Clean	23.53	4.35	5.69	1.37	1.28	0.21	0.05
	Polluted	68.98	24.87	14.63	0.87	0.62	0.40	0.09
	Whole-Min	18.32	2.37	2.33	0.30	0.19	0.09	0.02
	Whole-Max	143.10	73.47	22.06	2.02	1.96	0.59	0.13
	Whole-Mean	57.62	19.74	12.40	0.99	0.78	0.35	0.08

273 ^a represented the photolysis rate constant of particulate nitrate leading to HONO production after considering the
 274 influence of the shadowing effect. ^{b, c} represented the noontime source strength of HONO through the photolysis of
 275 particulate nitrate with the units of $10^{-5} \text{ mol h}^{-1} \text{ m}^{-2}$ and ppbv h^{-1} , respectively. ^{d, e} represented the minimum and
 276 maximum values of S_{HONO} during the observation period.
 277



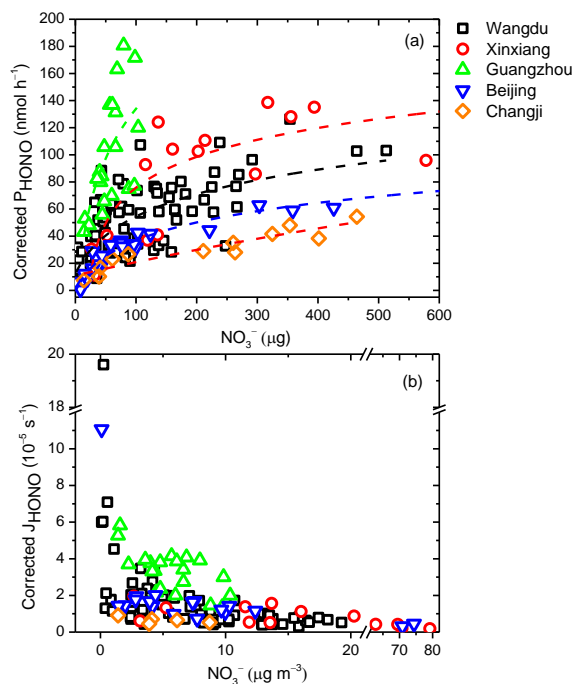


280 **Figure 5.** (a) Average corrected J_{HONO} , and (b) the ratio of OC to NO_3^- under different air conditions in
 281 five representative cities. The box represents the 25th to 75th percentiles, the horizon line represents
 282 the median, the hollow square represents the mean, and the 10th and the 90th percentiles are the bottom
 283 and top whiskers, respectively.

284 3.3 Dominant factors controlling J_{HONO}

285 3.3.1 Particulate nitrate

286 As shown in Table 1, the corrected J_{HONO} values varied with sampling periods and locations over a
 287 wide range, distributing from $0.16 \times 10^{-5} \text{ s}^{-1}$ for the aerosol sample collected in Changji with $\text{PM}_{2.5}$
 288 higher than $90 \mu\text{g m}^{-3}$, to $19.60 \times 10^{-5} \text{ s}^{-1}$ for the aerosol sample collected in Wangdu with $\text{PM}_{2.5}$ lower
 289 than $25 \mu\text{g m}^{-3}$. Several factors may contribute to the discrepancy of J_{HONO} in these different aerosol
 290 samples, such as particulate nitrate, organic matter, and aerosol acidity.



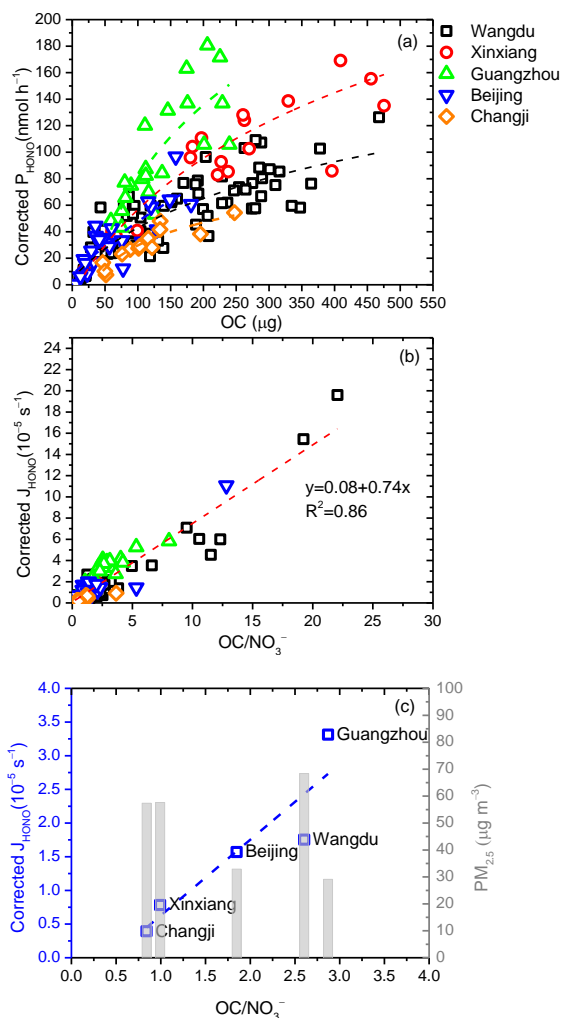
291
 292 **Figure 6.** Relationships between (a) corrected P_{HONO} and particulate nitrate loading, and (b) corrected
 293 J_{HONO} and particulate nitrate concentration in different sampling locations. The dash lines in (a) were
 294 the best fits to the data for the fitting equation: the aerosol samples in Guangzhou ($a=4.30$, $b=0.06$, $c=1$
 295 $\times 10^{-6}$, $R^2=0.42$), Wangdu ($a=2.54$, $b=0.11$, $c=1 \times 10^{-6}$, $R^2=0.50$), Beijing ($a=1.51$, $b=0.06$, $c=1 \times 10^{-6}$,



296 $R^2=0.91$), Xinxiang ($a=2.28$, $b=0.06$, $c=1\times 10^{-6}$, $R^2=0.47$), and Changji ($a=0.58$, $b=0.04$, $c=1\times 10^{-6}$,
297 $R^2=0.86$).

298 As shown in Figure 6, after considering the shadowing effect, the corrected P_{HONO} generally
299 increased along with the increased amount of particulate nitrate (pNO_3^- , μg), but still gradually slowed
300 down at high particulate nitrate loading, resulting in a rapid decrease in J_{HONO} . For example, when
301 NO_3^- concentration was at low level (around $0.5 \mu\text{g m}^{-3}$) in Wangdu, the value of corrected J_{HONO} was
302 about 30 times higher than that at high NO_3^- concentration (around $20 \mu\text{g m}^{-3}$). Previous works found
303 that the particulate nitrate was associated with matrix components in aerosol samples, and the
304 photolysis reactivity of particulate nitrate was closely associated with the surface catalysis effect (Ye et
305 al., 2017). In such a mechanism, the interaction between particulate nitrate and the substrate can distort
306 the molecular structure of nitrate and increase the absorption cross-section. The increases of P_{HONO} with
307 pNO_3^- exposed to the light radiation can be fitted by a logarithm curve under different
308 environment: $P_{\text{HONO}} = \frac{a}{b} \ln(1 + b(\text{pNO}_3^-)) + c(\text{pNO}_3^-)$ (Ye et al., 2017; Ye et al., 2019). Based on this
309 fitting equation, the corrected P_{HONO} as a function of pNO_3^- was showed in Figure 6a. Interestingly,
310 these relationships under different sampling locations showed distinct upward trends. Ye et al. (2019)
311 found that this ratio of a to b was related to the catalysis power of surface reactive sites and the organic
312 matters in the matrix. The much higher ratio of a (4.30) to b (0.06) values fitted for Guangzhou than
313 those for other cities, especially Changji ($a=0.58$, $b=0.04$), suggested extra catalytic power of organic
314 components in addition to the surface reactive site on particulate nitrate. The large deviation of the ratio
315 of a to b among these cities indicated the limitation of predicting P_{HONO} only based on the relationship
316 with particulate nitrate in different atmospheric environments, and other varied aerosol chemical and
317 physical conditions should be considered as well.

318 3.3.2 Organic matter



319

320

321 **Figure 7.** Relationship between (a) corrected P_{HONO} and OC loadings, (b) corrected J_{HONO} and OC/NO_3^- ,
 322 and (c) average corrected J_{HONO} , $\text{PM}_{2.5}$, and OC/NO_3^- during the sampling period in five representative
 323 cities.

324 Organic matter was ubiquitous in the atmosphere and contributed significantly to the total aerosol
 325 mass. The selectivity of organic matter that coexisted in the aerosols was very important for the
 326 production of HONO from the photolysis of particulate nitrate (Bao et al., 2018; Ye et al., 2016a;
 327 Svoboda et al., 2013; Reeser et al., 2013; Stemmler et al., 2006; Yang et al., 2018; Beine et al., 2006;
 328 Wang et al., 2021). As shown in Figure 7a, corrected P_{HONO} generally increased as the amount of OC in
 329 aerosol samples (pOC, μg) went up, while these positive correlations between P_{HONO} and pOC shown



330 may be due to the moderate correlation between pNO_3^- and pOC ($R^2=0.39$, Figure S3). To eliminate
331 the contribution from particulate nitrate, the dependence of J_{HONO} on the ratio of OC to NO_3^- (OC/NO_3^-)
332 was examined:

$$333 \text{ Corrected } J_{\text{HONO}} = 0.74 \times (\text{OC}/\text{NO}_3^-) + 0.08 \quad (6)$$

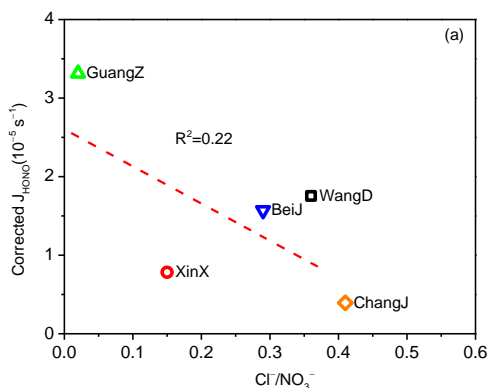
334 As shown in Figure 7b, significant linear correlation between corrected J_{HONO} and OC/NO_3^- was
335 found, with an R^2 of 0.86. In general, high corrected J_{HONO} values were mostly associated with high
336 OC/NO_3^- ratios for aerosol samples collected in the clean areas, such as Guangzhou, where the
337 averaged $\text{PM}_{2.5}$ level was the lowest (Figure 7c). Low corrected J_{HONO} values were mostly associated
338 with low OC/NO_3^- ratio, especially for aerosol samples collected in air polluted cities, such as Changji
339 and Xinxiang. However, Wangdu, a rural site in the North China Plain, where the $\text{PM}_{2.5}$ was dominated
340 by OM mainly due to local residential coal combustion (Liu et al., 2016; Li et al., 2024; Liu et al.,
341 2017), was an exception. As shown in Figure 5b, the OC/NO_3^- ratio in clean days was generally higher
342 than that in polluted conditions. Interestingly, different from other cities, the OC/NO_3^- ratio in
343 Guangzhou increased at polluted conditions, which was consistent with the correspondingly higher
344 corrected J_{HONO} value. Guangzhou was located in the PRD region, and was characterized by large
345 fractions of OM in $\text{PM}_{2.5}$ due to large emission of VOCs from numerous manufacturing industries and
346 transport-related sources (Zheng et al., 2009), and the water-soluble organic carbon (WSOC) was the
347 dominated component in the organic aerosols ($\text{WSOC}/\text{OC}=0.63$) (Chang et al., 2019). It's reported that
348 organic compounds on the surface may act as photosensitizers in the photolysis of particulate nitrate
349 (Gen et al., 2022; Handley et al., 2007; Cao et al., 2022; Wang et al., 2021). The association of
350 particulate nitrate with organic matter may distort its molecular structure and enhance the absorption
351 cross section, resulting in significantly enhancement in the photochemical production of HONO. The
352 organic matter can also become hydrogen donors, and directly transfer hydrogen from organic
353 H-donors to NO_2 to form HONO (Gen et al., 2022). Therefore, we suggested that the gradually
354 increasing role of organic matter in $\text{PM}_{2.5}$ in China should be of great concern.

355 3.3.3 Other factors

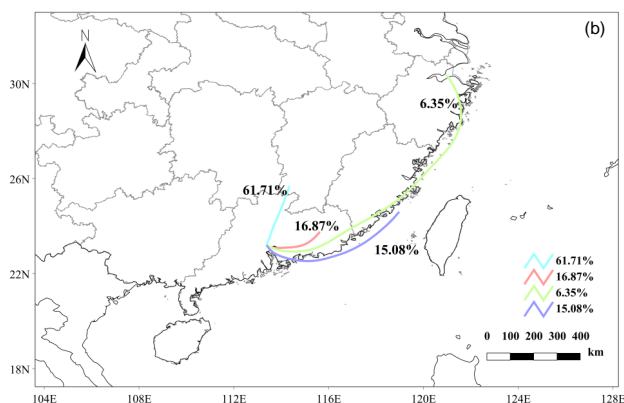
356 The acidic proton may play an important role in the photochemical production of HONO
357 and affect the release of photolysis products (Bao et al., 2018; Scharko et al., 2014). Scharko et al.
358 (2014) found that gaseous HONO production from nitrate photolysis was the highest at the lowest



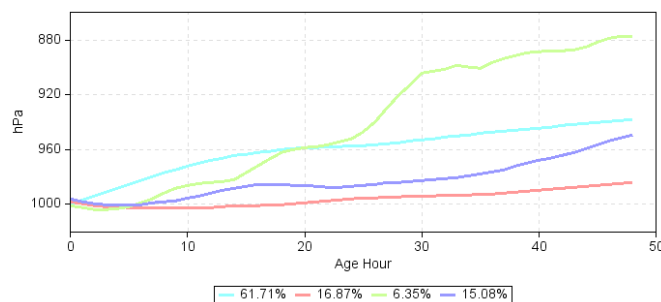
359 aerosol acidity (pH, ~2) and decreased with pH, and reached almost zero at pH higher than 4. In this
360 work, the estimated pH of these aerosol samples was in the range of 1.83–3.46 (the Extended Aerosol
361 Inorganic Model, E-AIM (Shi et al., 2021; Wexler and Clegg, 2002; Clegg et al., 1998)) with detailed
362 information provided in the Supporting Information. As shown in Figure S4, however, the correlation
363 between pH and J_{HONO} was weak, which indicated that pH was an important factor, but not the key one
364 driving the spatial differences of J_{HONO} in this work. Noting that halide ions, such as chlorine (Cl^-), may
365 lead to enhancement of surface nitrate anion and promote nitrate photolysis (Gen et al., 2022; Zhang et
366 al., 2020a), we also plotted J_{HONO} against the molar ratio of Cl^- to NO_3^- ($\text{Cl}^-/\text{NO}_3^-$) in Figure 8a. Even
367 though Guangzhou was a southern coastal city, the sampling site in this work was far away from the
368 South China Sea (>50 km). Besides, during the observation period, the aerosol collected in Guangzhou
369 was more representative of inland aerosol instead of marine aerosol, with the air parcel usually coming
370 from inland directions (Figure 8b) and the ratio of Cl^- to NO_3^- (0.02) much lower than that in fresh sea
371 spray aerosol (>1.0) (Xiao et al., 2017; Pipalatkhar et al., 2014; Atzei et al., 2019; Wang et al., 2019).
372 Therefore, we suggested that the halide ions were not the determining factor for the high J_{HONO} value in
373 Guangzhou, and the exact role of halide ions in HONO formation through the photolysis of particulate
374 nitrate required further investigation.



375



376



377

378 **Figure 8.** (a) Relationship between the average corrected J_{HONO} and $\text{Cl}^-/\text{NO}_3^-$ under different sampling
379 locations, and (b) the back trajectory cluster analysis in Guangzhou during the sampling period.

380 3.4 Environmental implication

381 The determined J_{HONO} was closely associated with the aerosol chemical and physical characteristics,
382 especially the coexisted organic components, and distributed around the curve as expressed by Eq. (6).
383 It's the first effort to explore the photolysis of particulate nitrate in aerosol samples collected from
384 different typical regions of China. The enhanced formation of HONO from the photolysis of particulate
385 nitrate can contribute significantly to the atmospheric oxidation capacity. To assess the photolysis of
386 particulate nitrate as a HONO daytime source, the noontime source strength of HONO (S_{HONO}) through
387 this mechanism in the air column within the planetary boundary layer can be calculated by the
388 following equation (Ye et al., 2017):

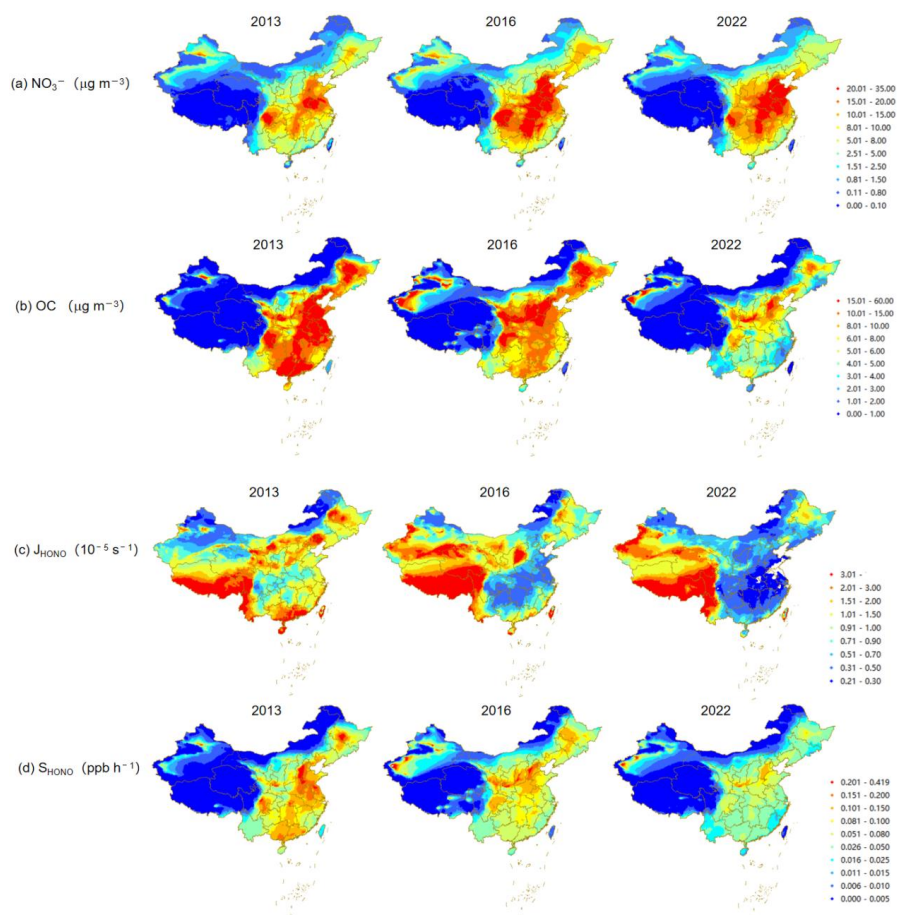
$$389 S_{\text{HONO}} (10^{-5} \text{ mol h}^{-1} \text{ m}^{-2}) = 0.67 \times \text{NO}_3^- (\mu\text{mol m}^{-3}) \times 10^{-6} \times J_{\text{HONO}} \times \text{BLH} \times 3600 \quad (7)$$

390 or

$$391 S_{\text{HONO}} (\text{ppbv h}^{-1}) = 0.67 \times \text{NO}_3^- (\text{ppbv}) \times J_{\text{HONO}} \times 3600 \quad (8)$$



392 where BLH means the boundary mixing height (m). Here, we assumed a typical BLH of 1000 m.
393 Based on the daily measured NO_3^- and corrected J_{HONO} value in each city, the S_{HONO} derived from Eq.
394 (7) or (8) during the observation period was showed in Table 1. It was found that, even though the
395 J_{HONO} in polluted days was much lower than that in clean days, due to the apparent higher NO_3^-
396 concentration, the corresponding S_{HONO} was about twice the average in clean days. The calculated
397 S_{HONO} ranged from $0.03 \times 10^{-5} \text{ mol h}^{-1} \text{ m}^{-2}$ to $0.88 \times 10^{-5} \text{ mol h}^{-1} \text{ m}^{-2}$ (0.01 ppbv h^{-1} – 0.2 ppbv h^{-1}), with
398 the mean value of $0.36 \times 10^{-5} \text{ mol h}^{-1} \text{ m}^{-2}$ (0.08 ppbv h^{-1}), which was comparable or higher than other
399 HONO sources (Bhattarai et al., 2019; Wang et al., 2023b; Ye et al., 2017). For example, the soil
400 HONO emission flux was measured in the range of $1.81 \times 10^{-6} \text{ mol h}^{-1} \text{ m}^{-2}$ – $4.55 \times 10^{-6} \text{ mol h}^{-1} \text{ m}^{-2}$ in
401 the soil without suffering nitrogen fertilizer (Bhattarai et al., 2019). The mean value of S_{HONO} during
402 the observation period was the highest in Wangdu ($0.42 \times 10^{-5} \text{ mol h}^{-1} \text{ m}^{-2}$, 0.10 ppbv h^{-1}) and
403 Guangzhou ($0.41 \times 10^{-5} \text{ mol h}^{-1} \text{ m}^{-2}$, 0.09 ppbv h^{-1}), followed by Xinxiang ($0.35 \times 10^{-5} \text{ mol h}^{-1} \text{ m}^{-2}$, 0.08
404 ppbv h^{-1}), Beijing ($0.22 \times 10^{-5} \text{ mol h}^{-1} \text{ m}^{-2}$, 0.05 ppbv h^{-1}), and Changji ($0.13 \times 10^{-5} \text{ mol h}^{-1} \text{ m}^{-2}$, 0.03
405 ppbv h^{-1}). Even though the $\text{PM}_{2.5}$ and NO_3^- concentration was the lowest in Guangzhou, the S_{HONO} was
406 much higher than other cities with air pollution. It should be noted that the S_{HONO} calculated with the
407 daily changed NO_3^- and J_{HONO} value in this work was much lower than the value reported by Bao et al.
408 (2018) (0.78 ppbv h^{-1}), which applied the average NO_3^- ($6.64 \mu\text{g m}^{-3}$, 2.62 ppbv) and the J_{HONO} range
409 ($1.22 \times 10^{-5} \text{ s}^{-1}$ – $4.84 \times 10^{-4} \text{ s}^{-1}$) to simulate S_{HONO} (0.12 ppbv h^{-1} – 4.57 ppbv h^{-1}). Other works, such as Fu
410 et al. (2019) and Gu et al. (2022a), applied the mean value of J_{HONO} ($8.3 \times 10^{-5} \text{ s}^{-1}$) and the observed
411 NO_3^- concentration to calculate S_{HONO} . However, due to the significant decrease of J_{HONO} along with
412 the increase of NO_3^- , the S_{HONO} calculated with mean NO_3^- or J_{HONO} will be largely overestimated, thus
413 directly influencing the identification of HONO sources. For example, J_{HONO} was the highest in
414 Wangdu in November 23, 2023 with the value of $19.6 \times 10^{-5} \text{ s}^{-1}$, while the corresponding NO_3^-
415 concentration was low ($0.39 \mu\text{g m}^{-3}$). If applying the average NO_3^- concentration ($12.53 \mu\text{g m}^{-3}$,
416 equivalent to 4.53 ppbv) and the maximum J_{HONO} value, the determined S_{HONO} value would be
417 $9.56 \times 10^{-5} \text{ mol h}^{-1} \text{ m}^{-2}$ (2.14 ppbv h^{-1}), which was about 30 times higher than the actual result (0.07
418 ppbv h^{-1}). Therefore, we suggested to estimate S_{HONO} with the observed concentration of NO_3^- and the
419 J_{HONO} value derived from the parameterization equation with OC/NO_3^- , thereby reducing the large
420 uncertainties and improving estimations of HONO budget.



421

422

423 **Figure 9.** Spatial distributions of the average (a) NO_3^- , (b) OC, (c) J_{HONO} and (d) S_{HONO} from
 424 November 15 to December 15 in the year of 2013, 2016, and 2022 in China. The J_{HONO} and S_{HONO}
 425 estimated in this work were derived under the same environmental conditions (RH=65 %,
 426 temperature=20 °C, and light intensity=150 kW m^{-2}), thus were more representative of the potential of
 427 HONO production rather than the actual value in the real ambient environment.

428 On the basis of the daily average concentrations of NO_3^- and OC extracted from the Chinese high
 429 resolution $\text{PM}_{2.5}$ Component simulation concentration dataset (CAQRA-aerosol,
 430 <https://www.capdatabase.cn>, 15 km×15 km) (Kong, et al., 2024), the J_{HONO} and S_{HONO} can be estimated
 431 by Eq. (6) and (8), respectively. As shown in Figure 9, significant spatio-temporal change
 432 characteristics of NO_3^- , OC, J_{HONO} and S_{HONO} were demonstrated in autumn-winter seasons from 2013
 433 to 2022 in China. The high J_{HONO} were concentrated in the ‘clean’ environments (e.g., Tibetan Plateau



434 area, South Xinjiang Basin, Yunnan-Guizhou plateaus, and Sichuan basins) and followed by those air
435 polluted regions (e.g., NCP, Fenhe-Weihe Basin, Northeastern China, and PRD). From 2013 to 2022,
436 with OC decreasing significantly, while NO_3^- keeping stable or even increasing, J_{HONO} showed a
437 downward trend in most regions. Although the J_{HONO} in polluted regions was comparatively lower than
438 that in ‘clean’ environments, the higher values of S_{HONO} were mostly distributed in these polluted
439 regions resulting from the much higher NO_3^- concentration. However, it should be noted that the
440 photolysis of particulate nitrate contributed only a small fraction to the needed daytime HONO source
441 in these polluted regions, such as 1.26–3.82 ppbv h^{-1} in the cities in the North China Plain (Hou et al.,
442 2016; Wang et al., 2017; Lian et al., 2022; Li et al., 2018), 0.75 ppbv h^{-1} in the Western China (Huang
443 et al., 2017), and 0.77–4.90 ppbv h^{-1} in Southern China (Li et al., 2012; Su et al., 2008). We noted that
444 uncertainties still exist in our simulations. Given the paucity of filed measurements of HONO
445 production from aerosol samples in ‘clean’ environments, the deviation of J_{HONO} derived from the
446 parametrization in this work may be large in these regions. Additionally, the concentrations of NO_3^-
447 and OC extracted from the CAQRA-aerosol in ‘clean’ environments were around the mean deviation
448 level. Therefore, more field observations and simulation experiments should be taken in these ‘clean’
449 regions in the future, to enrich and improve the parametric equations of J_{HONO} , and further evaluate the
450 contribution of nitrate photolysis to the formation of HONO in different regions in China.

451 **4 Conclusions**

452 This study for the first time systematically analyzed the production of HONO from the photolysis
453 of particulate nitrate in $\text{PM}_{2.5}$ samples from multiple sites across China, shedding light to the
454 contribution of this photolysis process to HONO daytime source in different environments. A total of
455 20 pairs of comparative photochemical experiments were conducted in Wangdu to evaluate and
456 quantify the shadowing effect. We found that the corrected J_{HONO} values varied with sampling periods
457 and locations over a wide range, distributing from $0.16 \times 10^{-5} \text{ s}^{-1}$ to $19.60 \times 10^{-5} \text{ s}^{-1}$. The coexisted
458 organic components in $\text{PM}_{2.5}$ can promote the photolysis of particulate nitrate, with higher J_{HONO}
459 generally associated with higher OC/ NO_3^- ratio. Considering the logarithmical decrease of J_{HONO} with
460 increased NO_3^- , we suggested that the S_{HONO} should be calculated with J_{HONO} derived from the
461 parameterization equation with OC/ NO_3^- instead of the average value. The photolysis of particulate



462 nitrate can become a potential daytime HONO source in southern urban cities, such as GuangZ, which
463 was characterized by large VOCs emissions and enhanced formation of secondary particulate
464 organic matter. Our work has provided an important reference for the research in other areas in the
465 world with high proportion of organic components in aerosol samples, such as United States
466 (Hass-Mitchell et al., 2024) and Europe (Bressi et al., 2021). To note, the filter samples collected in this
467 work may not cover all representative environments in China, especially the background sites, more
468 field observations and simulation experiments are needed in the future to better constrain the
469 parameterization and mechanism of particulate nitrate photolysis.



470 **Data availability.** The data used in this paper can be provided upon request from the corresponding
471 author.

472

473 **Author contributions.** J W, B L and K Z conceived the study and designed the experiments. J W, B
474 L, J G, C C, L W, Y Z, J L, Y Z, and X D analyzed the data. J W and B L prepared the manuscript
475 and all the coauthors helped improve the manuscript.

476

477 **Competing interests.** The authors declare that they have no conflict of interest.

478

479 **Acknowledgement.** We thank the Data Integration Program of the Major Research Plan of the
480 National Natural Science Foundation of China (No. 92044303, <https://www.cnpdatabase.cn>) for
481 making the high-resolution simulation dataset of PM_{2.5} chemical composition in Chinese from 2013 to
482 2020 available.

483

484 **Financial support.** This work was supported by the Central Level, Scientific Research Institutes for
485 Basic R&D Special Fund Business, China (No. 2022YSKY-26), and the National Key Research and
486 Development Program of China (No. 2022YFC3701100).



487 **References**

- 488 Ammann, M., Kalberer, M., Jost, D. T., Tobler, L., Rösler, E., Piguet, D., Gägeler, H. W., and
489 Baltensperger, U.: Heterogeneous production of nitrous acid on soot in polluted air masses, *Nature*,
490 395, 157-160, 10.1038/25965, 1998.
- 491 Andersen, S. T., Carpenter, L. J., Reed, C., Lee, J. D., Chance, R., Sherwen, T., Vaughan, A. R., Stewart,
492 J., Edwards, P. M., Bloss, W. J., Sommariva, R., Crilley, L. R., Nott, G. J., Neves, L., Read, K.,
493 Heard, D. E., Seakins, P. W., Whalley, L. K., Boustead, G. A., Fleming, L. T., Stone, D., and Fomba,
494 K. W.: Extensive field evidence for the release of HONO from the photolysis of nitrate aerosols, *Sci.*
495 *Adv.*, 9, eadd6266, doi:10.1126/sciadv.add6266, 2023.
- 496 Atzei, D., Fermo, P., Vecchi, R., Fantauzzi, M., Comite, V., Valli, G., Cocco, F., and Rossi, A.:
497 Composition and origin of PM_{2.5} in Mediterranean Countryside, *Environ. Pollut.*, 246, 294-302,
498 <https://doi.org/10.1016/j.envpol.2018.12.012>, 2019.
- 499 Bao, F., Li, M., Zhang, Y., Chen, C., and Zhao, J.: Photochemical aging of Beijing urban PM_{2.5}: HONO
500 production, *Environ. Sci. Technol.*, 52, 6309-6316, 10.1021/acs.est.8b00538, 2018.
- 501 Bao, F., Jiang, H., Zhang, Y., Li, M., Ye, C., Wang, W., Ge, M., Chen, C., and Zhao, J.: The key role of
502 sulfate in the photochemical renoxification on real PM_{2.5}, *Environ. Sci. Technol.*, 54, 3121-3128,
503 10.1021/acs.est.9b06764, 2020.
- 504 Beine, H. J., Amoroso, A., Domínguez, F., King, M. D., Nardino, M., Ianniello, A., and France, J. L.:
505 Surprisingly small HONO emissions from snow surfaces at Browning Pass, Antarctica, *Atmos.*
506 *Chem. Phys.*, 6, 2569-2580, 10.5194/acp-6-2569-2006, 2006.
- 507 Bhattarai, H. R., Liimatainen, M., Nykänen, H., Kivimäki, M., Martikainen, P. J., and Maljanen, M.:
508 Germinating wheat promotes the emission of atmospherically significant nitrous acid (HONO) gas
509 from soils, *Soil Biol. Biochem.*, 136, 10.1016/j.soilbio.2019.06.014, 2019.
- 510 Bressi, M., Cavalli, F., Putaud, J. P., Fröhlich, R., Petit, J. E., Aas, W., Äijälä, M., Alastuey, A., Allan, J.,
511 D., Aurela, M., Berico, M., Bougiatioti, A., Bukowiecki, N., Canonaco, F., Crenn, V., Dusanter, S.,
512 Ehn, M., Elsasser, M., Flentje, H., Graf, P., Green, D. C., Heikkinen, L., Hermann, H., Holzinger, R.,
513 Hueglin, C., Keernik, H., Kiendler-Scharr, A., Kubelová, L., Lunder, C., Maasikmets, M., Makeš, O.,
514 Malaguti, A., Mihalopoulos, N., Nicolas, J. B., O'Dowd, C., Ovadnevaite, J., Petralia, E., Poulain, L.,
515 Priestman, M., Riffault, V., Ripoll, A., Schlag, P., Schwarz, J., Sciare, J., Slowik, J., Sosedova, Y.,



- 516 Stavroulas, I., Teinemaa, E., Via, M., Vodička, P., Williams, P. I., Wiedensohler, A., Young, D. E.,
517 Zhang, S., Favez, O., Minguillón, M. C., and Prevot, A. S. H.: A European aerosol phenomenology -
518 7: High-time resolution chemical characteristics of submicron particulate matter across Europe,
519 Atmos. Environ.: X, 10, 10.1016/j.aeoa.2021.100108, 2021.
- 520 Cao, Y., Ma, Q., Chu, B., and He, H.: Homogeneous and heterogeneous photolysis of nitrate in the
521 atmosphere: state of the science, current research needs, and future prospects, Front. Env. Sci. Eng.,
522 17, 10.1007/s11783-023-1648-6, 2022.
- 523 Chang, D., Wang, Z., Guo, J., Li, T., Liang, Y., Kang, L., Xia, M., Wang, Y., Yu, C., Yun, H., Yue, D.,
524 and Wang, T.: Characterization of organic aerosols and their precursors in southern China during a
525 severe haze episode in January 2017, Sci. Total. Environ., 691, 101-111,
526 10.1016/j.scitotenv.2019.07.123, 2019.
- 527 Cheng, C., Yang, S., Yuan, B., Pei, C., Zhou, Z., Mao, L., Liu, S., Chen, D., Cheng, X., Li, M., Shao,
528 M., and Zhou, Z.: The significant contribution of nitrate to a severe haze event in the winter of
529 Guangzhou, China, Sci. Total. Environ., 909, 168582, 10.1016/j.scitotenv.2023.168582, 2024.
- 530 Clegg, S. L., Brimblecombe, P., and Wexler, A. S.: Thermodynamic Model of the System
531 $\text{H}^+ - \text{NH}_4^+ - \text{Na}^+ - \text{SO}_4^{2-} - \text{NO}_3^- - \text{Cl}^- - \text{H}_2\text{O}$ at 298.15 K, J. Phy. Chem. A, 102, 2155-2171,
532 10.1021/jp973043j, 1998.
- 533 Finlayson-Pitts, B. J. a. P. J., J. N.: Chemistry of the upper and lower atmosphere: theory, experiments,
534 and applications, Academic Press, San Diego, CA, xxii+969 pp., ISBN 0-12-257060-x, 2000.
- 535 Fu, X., Wang, T., Zhang, L., Li, Q., Wang, Z., Xia, M., Yun, H., Wang, W., Yu, C., Yue, D., Zhou, Y.,
536 Zheng, J., and Han, R.: The significant contribution of HONO to secondary pollutants during a
537 severe winter pollution event in southern China, Atmos. Chem. Phys., 19, 1-14,
538 10.5194/acp-19-1-2019, 2019.
- 539 Gelencsér, A., Hoffer, A., Kiss, G., Tombácz, E., Kurdi, R., and Bencze, L.: In-situ formation of
540 light-absorbing organic matter in cloud water, J. Atmos. Chem., 45, 25-33,
541 10.1023/A:1024060428172, 2003.
- 542 Gen, M., Liang, Z., Zhang, R., Go Mabato, B. R., and Chan, C. K.: Particulate nitrate photolysis in the
543 atmosphere, Environ. Sci.-Atmos., 2, 111-127, 10.1039/d1ea00087j, 2022.
- 544 Gu, R., Shen, H., Xue, L., Wang, T., Gao, J., Li, H., Liang, Y., Xia, M., Yu, C., Liu, Y., and Wang, W.:
545 Investigating the sources of atmospheric nitrous acid (HONO) in the megacity of Beijing, China, Sci.



- 546 Total Environ., 812, 10.1016/j.scitotenv.2021.152270, 2022a.
- 547 Gu, R., Wang, W., Peng, X., Xia, M., Zhao, M., Zhang, Y., Wang, Y., Liu, Y., Shen, H., Xue, L., Wang,
548 T., and Wang, W.: Nitrous acid in the polluted coastal atmosphere of the South China Sea: Ship
549 emissions, budgets, and impacts, *Sci. Total. Environ.*, 153692, 10.1016/j.scitotenv.2022.153692,
550 2022b.
- 551 Handley, S. R., Clifford, D., and Donaldson, D. J.: Photochemical loss of nitric acid on organic films: a
552 possible recycling mechanism for NO_x, *Environ. Sci. Technol.*, 41, 3898-3903, 10.1021/es062044z,
553 2007.
- 554 Hass-Mitchell, T., Joo, T., Rogers, M., Nault, B. A., Soong, C., Tran, M., Seo, M., Machesky, J. E.,
555 Canagaratna, M., Roscioli, J., Clafin, M. S., Lerner, B. M., Blomdahl, D. C., Misztal, P. K., Ng, N.
556 L., Dillner, A. M., Bahreini, R., Russell, A., Krechmer, J. E., Lambe, A., and Gentner, D. R.:
557 Increasing contributions of temperature-dependent oxygenated organic aerosol to summertime
558 particulate matter in New York City, *ACS Environ. Sci. Technol. Air*, 1, 113-128,
559 10.1021/acsestair.3c00037, 2024.
- 560 Hou, S., Tong, S., Ge, M., and An, J.: Comparison of atmospheric nitrous acid during severe haze and
561 clean periods in Beijing, China, *Atmos. Environ.*, 124, 199-206, 10.1016/j.atmosenv.2015.06.023,
562 2016.
- 563 Huang, R.-J., Yang, L., Cao, J., Wang, Q., Tie, X., Ho, K.-F., Shen, Z., Zhang, R., Li, G., Zhu, C.,
564 Zhang, N., Dai, W., Zhou, J., Liu, S., Chen, Y., Chen, J., and O'Dowd, C. D.: Concentration and
565 sources of atmospheric nitrous acid (HONO) at an urban site in Western China, *Sci. Total Environ.*,
566 593-594, 165-172, <https://doi.org/10.1016/j.scitotenv.2017.02.166>, 2017.
- 567 Kim, M. and Or, D.: Microscale pH variations during drying of soils and desert biocrusts affect HONO
568 and NH₃ emissions, *Nat. Commun.*, 10, 3944, 10.1038/s41467-019-11956-6, 2019.
- 569 Kurtenbach, R., Becker, K. H., Gomes, J. A. G., Kleffmann, J., Lürzer, J. C., Spittler, M., Wiesen, P.,
570 Ackermann, R., Geyer, A., and Platt, U.: Investigations of emissions and heterogeneous formation of
571 HONO in a road traffic tunnel, *Atmos. Environ.*, 35, 3385-3394,
572 [https://doi.org/10.1016/S1352-2310\(01\)00138-8](https://doi.org/10.1016/S1352-2310(01)00138-8), 2001.
- 573 Lee, J. D., Whalley, L. K., Heard, D. E., Stone, D., Dunmore, R. E., Hamilton, J. F., Young, D. E.,
574 Allan, J. D., Laufs, S., and Kleffmann, J.: Detailed budget analysis of HONO in central London
575 reveals a missing daytime source, *Atmos. Chem. Phys.*, 16, 2747-2764, 10.5194/acp-16-2747-2016,



- 576 2016.
- 577 Lei, K., Xiao, T., Jiang, Z., Zifa, W., Bing, L. I. U., Yuanyuan, Z. H. U., Lili, Z., Duohong, C., Ke, H.,
578 Huangjian, W., Qian, W. U., Jin, S., Yele, S., Zirui, L., Jinyuan, X., Dongsheng, J., and Mei, Z.:
579 High-resolution simulation dataset of hourly PM_{2.5} chemical composition in China (CAQRA-aerosol)
580 from 2013 to 2020, *Adv. Atmos. Sci.*, 10.1007/s00376-024-4046-5, 2024.
- 581 Li, D., Xue, L., Wen, L., Wang, X., Chen, T., Mellouki, A., Chen, J., and Wang, W.: Characteristics and
582 sources of nitrous acid in an urban atmosphere of northern China: Results from 1-yr continuous
583 observations, *Atmos. Environ.*, 182, 296-306, <https://doi.org/10.1016/j.atmosenv.2018.03.033>, 2018.
- 584 Li, W., Tong, S., Cao, J., Su, H., Zhang, W., Wang, L., Jia, C., Zhang, X., Wang, Z., Chen, M., and Ge,
585 M.: Comparative observation of atmospheric nitrous acid (HONO) in Xi'an and Xianyang located in
586 the GuanZhong basin of western China, *Environ. Pollut.*, 289, 117679,
587 10.1016/j.envpol.2021.117679, 2021.
- 588 Li, X., Brauers, T., Häsel, R., Bohn, B., Fuchs, H., Hofzumahaus, A., Holland, F., Lou, S., Lu, K. D.,
589 Rohrer, F., Hu, M., Zeng, L. M., Zhang, Y. H., Garland, R. M., Su, H., Nowak, A., Wiedensohler, A.,
590 Takegawa, N., Shao, M., and Wahner, A.: Exploring the atmospheric chemistry of nitrous acid
591 (HONO) at a rural site in Southern China, *Atmos. Chem. Phys.*, 12, 1497-1513,
592 10.5194/acp-12-1497-2012, 2012.
- 593 Li, Y., An, J., Min, M., Zhang, W., Wang, F., and Xie, P.: Impacts of HONO sources on the air quality
594 in Beijing, Tianjin and Hebei Province of China, *Atmos. Environ.*, 45, 4735-4744,
595 <https://doi.org/10.1016/j.atmosenv.2011.04.086>, 2011.
- 596 Li, Z., Ren, Z., Liu, C., Ning, Z., Liu, J., Liu, J., Zhai, Z., Ma, X., Chen, L., Zhang, Y., Bai, L., and
597 Kong, S.: Heterogeneous variations in wintertime PM_{2.5} sources, compositions and exposure risks at
598 urban/suburban rural/remote rural areas in the post COVID-19/Clean-Heating period, *Atmos.*
599 *Environ.*, 326, 120463, <https://doi.org/10.1016/j.atmosenv.2024.120463>, 2024.
- 600 Lian, C., Wang, W., Chen, Y., Zhang, Y., Zhang, J., Liu, Y., Fan, X., Li, C., Zhan, J., Lin, Z., Hua, C.,
601 Zhang, W., Liu, M., Li, J., Wang, X., An, J., and Ge, M.: Long-term winter observation of nitrous
602 acid in the urban area of Beijing, *J. Environ. Sci. (China)*, 114, 334-342, 10.1016/j.jes.2021.09.010,
603 2022.
- 604 Liang, Y., Zha, Q., Wang, W., Cui, L., Lui, K. H., Ho, K. F., Wang, Z., Lee, S., and Wang, T.: Revisiting
605 nitrous acid (HONO) emission from on-road vehicles: A tunnel study with a mixed fleet, *J. Air Waste*



- 606 Manage., 67, 797-805, 10.1080/10962247.2017.1293573, 2017.
- 607 Liao, S., Zhang, J., Yu, F., Zhu, M., Liu, J., Ou, J., Dong, H., Sha, Q., Zhong, Z., Xie, Y., Luo, H.,
608 Zhang, L., and Zheng, J.: High gaseous nitrous acid (HONO) emissions from light-duty diesel
609 vehicles, *Environ. Sci. Technol.*, 55, 200-208, 10.1021/acs.est.0c05599, 2021.
- 610 Liu, P., Zhang, C., Mu, Y., Liu, C., Xue, C., Ye, C., Liu, J., Zhang, Y., and Zhang, H.: The possible
611 contribution of the periodic emissions from farmers' activities in the North China Plain to
612 atmospheric water-soluble ions in Beijing, *Atmos. Chem. Phys.*, 16, 10097-10109,
613 10.5194/acp-16-10097-2016, 2016.
- 614 Liu, P., Zhang, C., Xue, C., Mu, Y., Liu, J., Zhang, Y., Tian, D., Ye, C., Zhang, H., and Guan, J.: The
615 contribution of residential coal combustion to atmospheric PM_{2.5} in northern China during winter,
616 *Atmos. Chem. Phys.*, 17, 11503-11520, 10.5194/acp-17-11503-2017, 2017.
- 617 Liu, Y., Lu, K., Li, X., Dong, H., Tan, Z., Wang, H., Zou, Q., Wu, Y., Zeng, L., Hu, M., Min, K.-E.,
618 Kecorius, S., Wiedensohler, A., and Zhang, Y.: A comprehensive model test of the HONO sources
619 constrained to field measurements at rural North China Plain, *Environ. Sci. Technol.*, 53, 3517-3525,
620 10.1021/acs.est.8b06367, 2019.
- 621 Melissa A, D.: Soil surface acidity plays a determining role in the atmospheric-terrestrial exchange of
622 nitrous acid, *Proc. Natl. Acad. Sci. U. S. A.*, 52, 18472-18477, 10.1073/pnas.1418545112, 2014.
- 623 Monge, M. E., D'Anna, B., Mazri, L., Giroir-Fendler, A., Ammann, M., Donaldson, D. J., and George,
624 C.: Light changes the atmospheric reactivity of soot, *Proc. Natl. Acad. Sci. U. S. A.*, 107, 6605-6609,
625 10.1073/pnas.0908341107, 2010.
- 626 Mora Garcia, S. L., Pandit, S., Navea, J. G., and Grassian, V. H.: Nitrous acid (HONO) formation from
627 the irradiation of aqueous nitrate solutions in the presence of marine chromophoric dissolved organic
628 matter: comparison to other organic photosensitizers, *ACS Earth Space Chem.*, 5, 3056-3064,
629 10.1021/acsearthspacechem.1c00292, 2021.
- 630 Oswald, R., Behrendt, T., Ermel, M., Wu, D., Su, H., Cheng, Y., Breuninger, C., Moravek, A., Mougin,
631 E., Delon, C., Loubet, B., Pommerening-Roser, A., Sorgel, M., Poschl, U., Hoffmann, T., Andreae,
632 M. O., Meixner, F. X., and Trebs, I.: HONO emissions from soil bacteria as a major source of
633 atmospheric reactive nitrogen, *Science*, 341, 1233-1235, 10.1126/science.1242266, 2013.
- 634 Pipalatkar, P., Khaparde, V. V., Gajghate, D. G., and Bawase, M. A.: Source apportionment of PM_{2.5}
635 using a CMB model for a centrally located Indian city, *Aerosol Air Qual. Res.*, 14, 1089-1099,



- 636 10.4209/aaqr.2013.04.0130, 2014.
- 637 Reeser, D. I., Kwamena, N.-O. A., and Donaldson, D. J.: Effect of organic coatings on gas-phase
638 nitrogen dioxide production from aqueous nitrate photolysis, *J. Phys. Chem. C*, 117, 22260-22267,
639 10.1021/jp401545k, 2013.
- 640 Ren, X., Harder, H., Martinez, M., Leshner, R. L., Oligier, A., Simpas, J. B., Brune, W. H., Schwab, J. J.,
641 Demerjian, K. L., He, Y., Zhou, X., and Gao, H.: OH and HO₂ Chemistry in the urban atmosphere of
642 New York City, *Atmos. Environ.*, 37, 3639-3651, [https://doi.org/10.1016/S1352-2310\(03\)00459-X](https://doi.org/10.1016/S1352-2310(03)00459-X),
643 2003.
- 644 Romer, P. S., Wooldridge, P. J., Crouse, J. D., Kim, M. J., Wennberg, P. O., Dibb, J. E., Scheuer, E.,
645 Blake, D. R., Meinardi, S., Brosius, A. L., Thames, A. B., Miller, D. O., Brune, W. H., Hall, S. R.,
646 Ryerson, T. B., and Cohen, R. C.: Constraints on aerosol nitrate photolysis as a potential source of
647 HONO and NO_x, *Environ. Sci. Technol.*, 52, 13738-13746, 10.1021/acs.est.8b03861, 2018.
- 648 Scharko, N. K., Berke, A. E., and Raff, J. D.: Release of nitrous acid and nitrogen dioxide from nitrate
649 photolysis in acidic aqueous solutions, *Environ. Sci. Technol.*, 48, 11991-12001, 10.1021/es503088x,
650 2014.
- 651 Shi, Q., Tao, Y., Krechmer, J. E., Heald, C. L., Murphy, J. G., Kroll, J. H., and Ye, Q.: Laboratory
652 investigation of renoxification from the photolysis of inorganic particulate nitrate, *Environ. Sci.*
653 *Technol.*, 55, 854-861, 10.1021/acs.est.0c06049, 2021.
- 654 Slater, E. J., Whalley, L. K., Woodward-Massey, R., Ye, C., Lee, J. D., Squires, F., Hopkins, J. R.,
655 Dunmore, R. E., Shaw, M., Hamilton, J. F., Lewis, A. C., Crilley, L. R., Kramer, L., Bloss, W., Vu, T.,
656 Sun, Y., Xu, W., Yue, S., Ren, L., Acton, W. J. F., Hewitt, C. N., Wang, X., Fu, P., and Heard, D. E.:
657 Elevated levels of OH observed in haze events during wintertime in central Beijing, *Atmos. Chem.*
658 *Phys.*, 20, 14847-14871, 10.5194/acp-20-14847-2020, 2020.
- 659 Stemmler, K., Ammann, M., Donders, C., Kleffmann, J., and George, C.: Photosensitized reduction of
660 nitrogen dioxide on humic acid as a source of nitrous acid, *Nature*, 440, 195-198,
661 10.1038/nature04603, 2006.
- 662 Su, H., Cheng, Y. F., Shao, M., Gao, D. F., Yu, Z. Y., Zeng, L. M., Slanina, J., Zhang, Y. H., and
663 Wiedensohler, A.: Nitrous acid (HONO) and its daytime sources at a rural site during the 2004
664 PRIDE-PRD experiment in China, *J. Geophys. Res. Atmos.*, 113, 10.1029/2007jd009060, 2008.
- 665 Su, H., Cheng, Y., Oswald, R., Behrendt, T., Trebs, I., Meixner, F. X., Andreae, M. O., Cheng, P., Zhang,



- 666 Y., and Pöschl, U.: Soil nitrite as a source of atmospheric HONO and OH radicals, *Science*, 333,
667 1616-1618, 10.1126/science.1207687, 2011.
- 668 Svoboda, O., Kubelová, L., and Slaviček, P.: Enabling forbidden processes: quantum and solvation
669 enhancement of nitrate anion UV absorption, *J. Phys. Chem. A*, 117, 12868-12877,
670 10.1021/jp4098777, 2013.
- 671 Villena, G., Wiesen, P., Cantrell, C. A., Flocke, F., Fried, A., Hall, S. R., Hornbrook, R. S., Knapp, D.,
672 Kosciuch, E., Mauldin, R. L., McGrath, J. A., Montzka, D., Richter, D., Ullmann, K., Walega, J.,
673 Weibring, P., Weinheimer, A., Staebler, R. M., Liao, J., Huey, L. G., and Kleffmann, J.: Nitrous acid
674 (HONO) during polar spring in Barrow, Alaska: A net source of OH radicals?, *J. Geophys. Res.*, 116,
675 10.1029/2011jd016643, 2011.
- 676 Wang, H., Ding, J., Xu, J., Wen, J., Han, J., Wang, K., Shi, G., Feng, Y., Ivey, C. E., Wang, Y., Nenes,
677 A., Zhao, Q., and Russell, A. G.: Aerosols in an arid environment: The role of aerosol water content,
678 particulate acidity, precursors, and relative humidity on secondary inorganic aerosols, *Sci. Total
679 Environ.*, 646, 564-572, <https://doi.org/10.1016/j.scitotenv.2018.07.321>, 2019.
- 680 Wang, J., Zhang, X., Guo, J., Wang, Z., and Zhang, M.: Observation of nitrous acid (HONO) in Beijing,
681 China: Seasonal variation, nocturnal formation and daytime budget, *Sci. Total Environ.*, 587-588,
682 350-359, 10.1016/j.scitotenv.2017.02.159, 2017.
- 683 Wang, J., Gao, J., Che, F., Wang, Y., Lin, P., and Zhang, Y.: Decade-long trends in chemical component
684 properties of PM_{2.5} in Beijing, China (2011-2020), *Sci. Total Environ.*, 832, 154664,
685 10.1016/j.scitotenv.2022.154664, 2022a.
- 686 Wang, J., Gao, J., Che, F., Wang, Y., Lin, P., and Zhang, Y.: Dramatic changes in aerosol composition
687 during the 2016-2020 heating seasons in Beijing-Tianjin-Hebei region and its surrounding areas: The
688 role of primary pollutants and secondary aerosol formation, *Sci. Total. Environ.*, 849, 157621,
689 10.1016/j.scitotenv.2022.157621, 2022b.
- 690 Wang, J., Zhang, Y., Zhang, C., Wang, Y., Zhou, J., Whalley, L. K., Slater, E. J., Dyson, J. E., Xu, W.,
691 Cheng, P., Han, B., Wang, L., Yu, X., Wang, Y., Woodward-Massey, R., Lin, W., Zhao, W., Zeng, L.,
692 Ma, Z., Heard, D. E., and Ye, C.: Validating HONO as an intermediate tracer of the external cycling
693 of reactive nitrogen in the background atmosphere, *Environ. Sci. Technol.*, 57, 5474-5484,
694 10.1021/acs.est.2c06731, 2023a.
- 695 Wang, Y., Fu, X., Wang, T., Ma, J., Gao, H., Wang, X., and Pu, W.: Large contribution of nitrous acid to



- 696 soil-emitted reactive oxidized nitrogen and its effect on air quality, *Environ. Sci. Technol.*, 57,
697 3516-3526, 10.1021/acs.est.2c07793, 2023b.
- 698 Wang, Y., Xiao, S., Zhang, Y., Chang, H., Martin, R. V., Van Donkelaar, A., Gaskins, A., Liu, Y., Liu, P.,
699 and Shi, L.: Long-term exposure to PM_{2.5} major components and mortality in the southeastern
700 United States, *Environ. Int.*, 158, 106969, 10.1016/j.envint.2021.106969, 2022c.
- 701 Wang, Y., Huang, D. D., Huang, W., Liu, B., Chen, Q., Huang, R., Gen, M., Mabato, B. R. G., Chan, C.
702 K., Li, X., Hao, T., Tan, Y., Hoi, K. I., Mok, K. M., and Li, Y. J.: Enhanced nitrite production from
703 the aqueous photolysis of nitrate in the presence of vanillic acid and implications for the roles of
704 light-absorbing organics, *Environ. Sci. Technol.*, 55, 15694-15704, 10.1021/acs.est.1c04642, 2021.
- 705 Wang, Z., Zhang, D., Liu, B., Li, Y., Chen, T., Sun, F., Yang, D., Liang, Y., Chang, M., Yang, L., and
706 Lin, A.: Analysis of chemical characteristics of PM_{2.5} in Beijing over a 1-year period, *J. Atmos.*
707 *Chem.*, 73, 407-425, 10.1007/s10874-016-9334-8, 2016.
- 708 Wexler, A. S. and Clegg, S. L.: Atmospheric aerosol models for systems including the ions H⁺, NH₄⁺,
709 Na⁺, SO₄²⁻, NO₃⁻, Cl⁻, Br⁻, and H₂O, *J. Geophys. Res. Atmos.*, 107, ACH 14-1-ACH 14-14,
710 <https://doi.org/10.1029/2001JD000451>, 2002.
- 711 Xiao, H. W., Xiao, H. Y., Luo, L., Shen, C. Y., Long, A. M., Chen, L., Long, Z. H., and Li, D. N.:
712 Atmospheric aerosol compositions over the South China Sea: temporal variability and source
713 apportionment, *Atmos. Chem. Phys.*, 17, 3199-3214, 10.5194/acp-17-3199-2017, 2017.
- 714 Yang, W., Han, C., Yang, H., and Xue, X.: Significant HONO formation by the photolysis of nitrates in
715 the presence of humic acids, *Environ. Pollut.*, 243, 679-686, 10.1016/j.envpol.2018.09.039, 2018.
- 716 Ye, C., Gao, H., Zhang, N., and Zhou, X.: Photolysis of nitric acid and nitrate on natural and artificial
717 surfaces, *Environ. Sci. Technol.*, 50, 3530-3536, 10.1021/acs.est.5b05032, 2016a.
- 718 Ye, C., Zhang, N., Gao, H., and Zhou, X.: Photolysis of particulate nitrate as a source of HONO and
719 NO_x, *Environ. Sci. Technol.*, 51, 6849-6856, 10.1021/acs.est.7b00387, 2017.
- 720 Ye, C., Zhang, N., Gao, H., and Zhou, X.: Matrix effect on surface-catalyzed photolysis of nitric acid,
721 *Sci. Rep.*, 9, 4351, 10.1038/s41598-018-37973-x, 2019.
- 722 Ye, C., Zhou, X., Pu, D., Stutz, J., Festa, J., Spolaor, M., Tsai, C., Cantrell, C., Mauldin, R. L., Campos,
723 T., Weinheimer, A., Hornbrook, R. S., Apel, E. C., Guenther, A., Kaser, L., Yuan, B., Karl, T.,
724 Haggerty, J., Hall, S., Ullmann, K., Smith, J. N., Ortega, J., and Knote, C.: Rapid cycling of reactive
725 nitrogen in the marine boundary layer, *Nature*, 532, 489-491, 10.1038/nature17195, 2016b.



- 726 Zhang, L., Wang, T., Zhang, Q., Zheng, J., Xu, Z., and Lv, M.: Potential sources of nitrous acid (HONO)
727 and their impacts on ozone: A WRF-Chem study in a polluted subtropical region, *J. Geophys. Res.*
728 *Atmos.*, 121, 3645-3662, <https://doi.org/10.1002/2015JD024468>, 2016.
- 729 Zhang, R., Gen, M., Huang, D., Li, Y., and Chan, C. K.: Enhanced sulfate production by nitrate
730 photolysis in the presence of halide ions in atmospheric particles, *Environ. Sci. Technol.*, 54,
731 3831-3839, [10.1021/acs.est.9b06445](https://doi.org/10.1021/acs.est.9b06445), 2020a.
- 732 Zhang, W., Tong, S., Jia, C., Wang, L., Liu, B., Tang, G., Ji, D., Hu, B., Liu, Z., Li, W., Wang, Z., Liu,
733 Y., Wang, Y., and Ge, M.: Different HONO sources for three layers at the urban area of Beijing,
734 *Environ. Sci. Technol.*, 54, 12870-12880, [10.1021/acs.est.0c02146](https://doi.org/10.1021/acs.est.0c02146), 2020b.
- 735 Zheng, J., Shao, M., Che, W., Zhang, L., Zhong, L., Zhang, Y., and Streets, D.: Speciated VOC
736 emission inventory and spatial patterns of ozone formation potential in the Pearl River Delta, China,
737 *Environ. Sci. Technol.*, 43, 8580-8586, [10.1021/es901688e](https://doi.org/10.1021/es901688e), 2009.
- 738 Zhou, X., Gao, H., He, Y., Huang, G., Bertman, S. B., Civerolo, K., and Schwab, J.: Nitric acid
739 photolysis on surfaces in low-NO_x environments: Significant atmospheric implications, *Geophys.*
740 *Res. Lett.*, 30, <https://doi.org/10.1029/2003GL018620>, 2003.
- 741 Zhou, X., Zhang, N., TerAvest, M., Tang, D., Hou, J., Bertman, S., Alaghmand, M., Shepson, P. B.,
742 Carroll, M. A., Griffith, S., Dusanter, S., and Stevens, P. S.: Nitric acid photolysis on forest canopy
743 surface as a source for tropospheric nitrous acid, *Nat. Geosci.*, 4, 440-443, [10.1038/ngeo1164](https://doi.org/10.1038/ngeo1164), 2011.